now published as: G. Skacej and C. Zannoni, Macromolecules, 47, 8824-8832 (2014)

Molecular simulations shed light on supersoft elasticity in polydomain liquid crystal elastomers

Gregor Skačej*,†,‡ and Claudio Zannoni¶

University of Ljubljana, NAMASTE Centre of Excellence, and University of Bologna

E-mail: gregor.skacej@fmf.uni-lj.si

Abstract

Liquid crystal elastomers (LCE) — polymer networks constructed with liquid crystal units — are functional materials characterized by a pronounced coupling between elastic strain and liquid crystalline orientational ordering. When prepared by polymerization and cross-linking in the isotropic phase, and then cooled ("isotropic-genesis"), a polydomain LCE presents an extraordinary "supersoft" elastic behavior under unidirectional pulling, with a plateau-like low elastic modulus region in the stress-strain curve, before turning into a monodomain LCE where a standard elastic resistance is recovered. The physical mechanism of this behavior is of great interest, but still mysterious. This work investigates its origin, reproducing the experiment and succeeding to observe the plateau-like stress-strain behavior by means of large-scale molecular isostress Monte Carlo simulations. The results show that the basic molecular mechanism behind supersoft elasticity hinges on local domain rotation and growth, but also suggest that this is assisted by a newly proposed dissipation of the elastic energy stored in

*To whom correspondence should be addressed

†Faculty of Mathematics and Physics, University of Ljubljana, Jadranska 19, SI-1000 Ljubljana, Slovenia

‡NAMASTE Centre of Excellence, Jamova 39, SI-1000 Ljubljana

¶Dipartimento di Chimica Industriale "Toso Montanari" and INSTM, Università di Bologna, Viale Risorgimento 4, I-40136 Bologna, Italy

the defects created by the isotropic genesis process, explaining also the irreversibility observed in main-chain LCE.

1 Introduction

Liquid crystal elastomers (LCE)[1] are fascinating functional materials with exciting applications in a variety of fields, ranging from nano- and microactuators,[2–7] biocompatible artificial muscles,[8–14] micropumps,[15] switchable gecko pad-like attach-detach surfaces,[16] haptic interfaces[2,17] and light-governable swimmers[18] to adaptive optical devices,[19] stretchable photonic crystals[20] and solar energy motors.[21] They consist of sparsely crosslinked polymeric networks with embedded mesogenic molecules either belonging to the polymer backbone (main-chain LCE), or attached to it (side-chain LCE). LCE can form isotropic, nematic, and smectic phases, and, being characterized by a pronounced coupling of strain and mesogenic alignment,[22] can respond to external stimuli such as temperature changes, ultra-violet light, or external (mechanical or electrical) fields by large (up to several 100%) elastic deformations. The properties of LCE depend critically on their preparation strategy. The synthesis process of a LCE sample from single monomers normally consists of two polymerization stages, the first generating the polymer strands and the second crosslinking them.[23] If a suitable external field is applied during the second polymerization step, a monodomain sample can be obtained, with uniform alignment of the average mesogenic orientation — the director. On the contrary, if no such precautions are taken, a polydomain sample is obtained, with micron-sized regions of uniform director, resulting in pronounced light scattering and an opaque sample appearance.[23]

The macroscopic behavior of monodomain LCE systems is well established and a successful continuum theoretical model — the so-called neoclassical model of Gaussian chains,[1,24] as well as mathematically rigorous[25] approaches based on laminate director structures, have been developed. More recently, several molecular-level off-lattice computer simulations have

been performed, providing useful insights into monodomain LCE,[26–29] including their actuation.[30] On the other hand, polydomain LCE are much less understood and deeply intriguing. Theoretically, the polydomain LCE ground state has been attributed to quenched orientational disorder due to anisotropic and essentially frozen crosslinks.[31–33] Upon unidirectional stretching a polydomain LCE is eventually transformed into a well-aligned and transparent monodomain sample,[33] but the miscroscopic mechanism — compatible with the spatial and orientational distribution of domains — is still unclear. The corresponding stress-strain behavior depends on sample preparation history and may differ significantly from that of an ordinary rubber. For example, nematic polydomain elastomers crosslinked while in the isotropic phase (I-PDE) exhibit a stress-strain curve with a characteristic plateau corresponding to supersoft elastic deformations that require vanishingly little work, while samples crosslinked in the aligned nematic phase (N-PDE) exhibit a more standard, Hookean, response.[34–38] There are examples of reversible[35,39] and irreversible[40–44] stress-strain behavior. The microstructure of both polydomain sample types consists of an isotropic distribution of ordered domains, which are typically smaller for the I-PDE than for the N-PDE.

Given all these issues, computer simulations would indeed seem a natural approach to investigate polydomain LCE, and help elucidate the miscoscopic origin and workings of supersoft elasticity. Here, however, significant difficulties exist with properly mimicking experimental conditions: To begin with, very large samples need to be prepared to replicate an overall isotropic polydomain structure with local orientational order. Moreover, the isotropic genesis procedure, which seems essential to observe the phenomenon experimentally, has to be reproduced somehow in simulations too. A recent molecular dynamics simulation work[45] has dealt with the polydomain-monodomain transformation of a smectic side-chain LCE characterized by an ideal tetrahedral topology and an entanglement-free polymer network. Equilibrium stress-strain behavior appeared to be similar to Hookean (plateau-less), observed experimentally in N-PDE samples,[35] even though it is not obvious whether the simulated system can be classified as N-PDE or I-PDE, as the sample preparation did not follow a

polymerization route.

While the possibility of obtaining large strain deformations with very small stress in I-PDE is of obvious importance for potential applications, understanding how this happens at molecular level still represents a major unanswered question. Therefore, we here present a large-scale molecular Monte Carlo (MC) simulation of swollen isotropic-genesis main-chain LCE, attempting to reproduce the soft plateau in the equilibrium stress-strain curve previously unseen in computer simulations. We build on our previous work[28,30] on thermal and electric actuation in regular swollen[35,46] monodomain main-chain LCE, explicitly following a simple double polymerization protocol and also exploring the polydomain LCE ground state itself. Analysis of our results allows us to examine various possible mechanisms for the poly-to-monodomain transformation, suggesting the most likely one(s). The rest of the paper is organized as follows: In Section 2 we present our strategy to prepare well-defined isotropic-genesis polydomains. In Section 3 we describe in detail the methodologies used for the simulations and for analyzing the huge raw data output in terms of meaningful quantities such as order parameters and local domain properties. These results are then presented in Section 4 and discussed in Section 5, while in Section 6 our conclusions are summarized.

2 Sample genesis

Our main chain LCE networks are obtained by polymerizing elongated mesogenic monomers of uniaxial ellipsoidal shape (σ_s wide and $\sigma_e = 3\sigma_s$ long), interacting via a soft Gay-Berne (GB) potential.[47] The original GB potential[48] promotes parallel side-to-side molecular alignment, which is essential for the formation of liquid-crystalline phases. The GB potential parametrization used here still ensures a rather wide nematic range,[49] while its soft-core modification facilitates MC equilibration, even for rather dense polymers.[28,30] The bonds between ellipsoids established upon polymerization are modeled by the Finitely Extensible Nonlinear Elastic (FENE) potential[50] applied both to bond stetching and bending (for more

details see Section 3). All monomers are endowed with two reactive bonding sites at particle ends[51,52] that, upon polymerization, provide the main chain strands. Monomers also exploit an additional reactive site on the equator whenever necessary for crosslinking.

Most of our stress-strain simulations are launched from so-called "reference" samples prepared in a cubic simulation box with periodic boundary conditions. In our polymerization protocol, first the polymer chains are grown at low density, each starting from random coordinates, along a randomly oriented straight line. In each growth step, chains are terminated with a probability of 0.125, yielding polydisperse strands $\sim 8 \pm 7.5$ monomers long. Once this first polymerization stage is completed, reticulation is performed by transversally connecting the active head/tail site of each terminal monomer to the nearest available equatorial site belonging to another chain [Figure 1 (a,b)]. This produces a highly interconnected and, compatibly with sample size, almost isotropic polymer network. The sample is then soaked with swelling monomers (51.5% volume fraction) to mimic experimental systems,[35,46] as well as to enhance polymer network mobility,[28,30] and isotropically compressed in a MC run at a nematic temperature. This increases the density ~ 25 times to $\rho^* = N\sigma_s^3/V \approx 0.287$, almost reaching close-packing. (Here, N denotes the total number of ellipsoids and V stands for sample volume.)

This preparation procedure should not impose any preferential polymer chain orientation prior to crosslinking and produce a nematic phase only after reticulation (as for I-PDE genesis conditions). The resulting polymer network is rather irregular and somewhat entangled; see Figure 1 (a). However, in any finite-size sample residual orientational order associated with incomplete averaging out is expected to exist. While the average polymer chain length approaches 8 monomers, several chains are only 1 unit long and represent, with their adjacent crosslinkers, small molecular clusters [like the one marked by a dashed circle in Figure 1 (b)] that may be difficult to reorient, acting as potential anisotropic sources of quenched disorder.[31,33]

To examine finite-size effects we considered different samples containing $N = 8000$, 64000,

and 216000 GB ellipsoids, all with periodic boundary conditions. Note that we here study samples with the same swelling monomer content as in Refs.,[28,30] but with a somewhat higher crosslink fraction ($\sim 12\%$) and a more irregular network architecture. The system evolution is studied through isostress Monte Carlo (MC) simulations,[28,30,53] performing the simulation equivalent of typical experiments such as temperature scans and stress-strain runs.

3 Simulation and analysis methods

3.1 Soft-core Gay-Berne interaction

Liquid crystal molecules (bonded or non-bonded) are represented by uniaxial ellipsoids. For a pair of ellipsoids whose long axes are given by unit vectors $\mathbf{u}_i$ and $\mathbf{u}_j$, with centers of mass separated by $\mathbf{r}_{ij}$ ($r_{ij} = |\mathbf{r}_{ij}|$, $\hat{\mathbf{r}}_{ij} = \mathbf{r}_{ij}/r_{ij}$), the original GB interaction energy reads[48]

$$U_{ij}^{GB} = 4\epsilon_{ij}\Big\{ \Big[\frac{\sigma_s}{r_{ij} - \sigma_{ij} + \sigma_s}\Big]^{12} - \Big[\frac{\sigma_s}{r_{ij} - \sigma_{ij} + \sigma_s}\Big]^{6} \Big\}. \tag{1}$$

Here $\sigma_{ij} = \sigma_s \Omega(\chi, \mathbf{u}_i, \mathbf{u}_j, \hat{\mathbf{r}}_{ij})^{-1/2}$, the core-range parameter, where

$$\Omega(\chi, \mathbf{u}_i, \mathbf{u}_j, \hat{\mathbf{r}}_{ij}) = 1 - \frac{\chi}{2}\Big[\frac{(\mathbf{u}_i \cdot \hat{\mathbf{r}}_{ij} + \mathbf{u}_j \cdot \hat{\mathbf{r}}_{ij})^2}{1 + \chi(\mathbf{u}_i \cdot \mathbf{u}_j)} + \frac{(\mathbf{u}_i \cdot \hat{\mathbf{r}}_{ij} - \mathbf{u}_j \cdot \hat{\mathbf{r}}_{ij})^2}{1 - \chi(\mathbf{u}_i \cdot \mathbf{u}_j)}\Big], \tag{2}$$

$\chi = (\kappa^2 - 1)/(\kappa^2 + 1)$, and $\kappa = \sigma_e/\sigma_s$. σ_e and σ_s denote the molecular length and width, respectively. — The energy parameter $\epsilon_{ij} = \epsilon(\epsilon'_{ij})^{\mu}(\epsilon''_{ij})^{\nu}$ takes into account attractive force anisotropy. ϵ stands for a characteristic GB interaction energy, μ and ν are dimensionless quantities; $\epsilon'_{ij} = \Omega(\chi', \mathbf{u}_i, \mathbf{u}_j, \hat{\mathbf{r}}_{ij})$ and $\epsilon''_{ij} = [1 - \chi^2(\mathbf{u}_i \cdot \mathbf{u}_j)^2]^{-1/2}$. Here $\chi' = (\kappa'^{1/\mu} - 1)/(\kappa'^{1/\mu} + 1)$ and $\kappa' = \epsilon_s/\epsilon_e$, with ϵ_s and ϵ_e denoting the attractive well depths for the side-by-side and end-to-end ellipsoidal pair configurations, respectively. — In the modified soft-core (SC) potential the strong GB repulsion is replaced by a weaker linear potential $U_{ij}^{SC} = m\,(r_{ij} - \sigma_{ij})$;[47] here m determines the linear slope. To keep the attractive features of the original GB potential, the GB and SC potentials are blended continuously, yielding $U_{ij}^{GBS} =$

$(1-f_{ij})U_{ij}^{GB} + f_{ij}U_{ij}^{SC}$, where $f_{ij} = 1/\{1+\exp[n(\sigma_{ij}-r_{ij})]\}$. — We use $\mu = 1$, $\nu = 3$, $\sigma_e/\sigma_s = 3$, $\epsilon_s/\epsilon_e = 5$ (providing a broad enough nematic region in the phase diagram), $m = -70\,\epsilon/\sigma_s$, and $n = -100/\sigma_s$.[28,47] For a typical prolate mesogen $\sigma_s \approx 5 \times 10^{-10}$ m and $\epsilon = \epsilon_s \approx 1.38 \times 10^{-21}$ J. A reduced temperature scale is introduced as $T^* = k_B T/\epsilon$.

3.2 Finitely Extensible Nonlinear Elastic potential

Consider a bond connecting two adjacent ellipsoids, with length s_{ij}, a deviation δs_{ij} from equilibrium value s_e ($\delta s_{ij} = |s_{ij} - s_e|$), and a limitation that $\delta s_{ij} < \delta s_m$. Similarly, let the bond angle θ_{ij} be measured between the preferred bond directions imposed by the ellipsoids.[51] The deviation from its equilibrium value θ_e is denoted by $\delta\theta_{ij} = |\theta_{ij} - \theta_e|$, with $\delta\theta_{ij} < \delta\theta_m$. Then, the bond energy can be written as[51,52]

$$U_{ij}^{FENE} = -k_s \delta s_m^2 \log\left[1 - \frac{\delta s_{ij}^2}{\delta s_m^2}\right] - k_\theta \delta\theta_m^2 \log\left[1 - \frac{\delta\theta_{ij}^2}{\delta\theta_m^2}\right]. \tag{3}$$

The two terms refer to bond stretching and bending. The preferred bond directions are parallel to the long and short ellipsoid axes for bonding sites at ellipsoid ends and on the equator, respectively. Here $s_e = 0.15\,\sigma_s$, $\delta s_m = 0.25\,\sigma_s$, and $k_s = 500\,\epsilon/\sigma_s^2 \approx 2.76$ Nm^{-1} for stretching, and $\theta_e = 0°$, $\delta\theta_m = 150°$, and $k_\theta = 3.8 \times 10^{-4}\epsilon\,\mathrm{deg}^{-2} \approx 1.72 \times 10^{-21}$ Jrad^{-2} for bending.[28,30,51,52]

3.3 Isostress Monte Carlo simulations

The interaction energy of N particles is obtained by summing up all intermolecular contributions $U = \sum_{i=1}^{N}\sum_{j=i+1}^{N}(U_{ij}^{GBS} + w_{ij}U_{ij}^{FENE})$, where $w_{ij} = 1$ if the ellipsoids i and j are bonded, and $w_{ij} = 0$ otherwise. The computational effort is reduced using Verlet neighbor lists[54] and cell linked-lists during neighbor list updates.[55] The interaction and neighbor list cutoffs are at $4\,\sigma_s$ and $5\,\sigma_s$, respectively. The overall computational cost scales approximately linearly with N, and parallelization is employed to provide additional speedup. — In

isotress MC simulations we follow a modified Metropolis algorithm,[28,53] performing different trial move types: *Translational moves.* Random displacement of an ellipsoid. *Rotational moves.* Random ellipsoid rotation with respect to a randomly selected Cartesian axis.[56] *Bonded pair rotations.* Affect only bonded bifunctional ellipsoids, excluding crosslinks; the selected particle pair is rotated by a random angle about an axis connecting the far-away pair ends. *Resize moves.* Collective trial moves involving all ellipsoids: two simulation box sides are chosen at random, each of them to undergo a different random variation; the third box side is determined by the incompressibility constraint. — One MC cycle consists of attempting translational and rotational moves for each ellipsoid, and bonded pair rotations for all eligible pairs. Moreover, every 5 cycles a resize move is attempted. The proposed move, resulting in energy change ΔU and deformation $\Delta\lambda_z$ along the z-axis, is accepted with probability $\min\{1, \exp\left[-(\Delta U - \Sigma_{zz} V \Delta\lambda_z)/k_B T\right]\}$,[28,53] where V denotes sample volume, T temperature, and Σ_{zz} external engineering stress. Trial move amplitudes are adjusted dynamically, ensuring acceptance ratios between 45% and 55%. Verlet neighbor lists are refreshed after every cycle (for $T^* \leq 3.0$ every 5 cycles), while the cell-linked lists are updated every 5000 cycles. Reduced stress is defined as $\sigma^* = \Sigma_{zz}\sigma_s^3/\epsilon$. — Equilibration run lengths range from ~ 4 to ~ 50 MC Mcycles, while typical production runs are 1 or 2 Mcycles long. Normally, MC runs at given conditions are launched directly from reference samples. Alternatively, this is done from configurations pre-equilibrated at a similar value of T^* or σ^*, if available, e.g., to speed up the slow relaxation of smectic phases.

3.4 Determination of orientational order

Orientational order of the ith elongated non-polar molecule (ellipsoid) is quantified by the second-rank ordering matrix $\mathsf{Q}_i = (3\mathbf{u}_i \otimes \mathbf{u}_i - \mathsf{I})/2$. In each MC cycle, we diagonalize the sample-averaged $\langle \mathsf{Q}_i \rangle_i$, including bonded and swelling ellipsoids, and obtain the corresponding largest eigenvalue. These are then averaged over all production MC cycles to give S_G, the global order parameter. — As for the order of individual ellipsoids in their local sur-

rounding, we average the ordering matrix of each particle over MC cycles to get $\langle \mathsf{Q}_i \rangle_{MC}$ and diagonalize it. The resulting largest eigenvalues are averaged over all particles, yielding the local order parameter S_L. — Similarly, an order parameter measuring order with respect to a fixed axis (say, z) is introduced as $S_z = [3\langle(\mathbf{u}_i \cdot \mathbf{z})^2\rangle_i - 1]/2$, where $\mathbf{z}$ denotes a unit vector along z.

3.5 Snapshot coarse-graining and domain properties

Molecular snapshot coarse-graining is convenient for an easier visualization of large samples. First, we split our samples into a mesh of $\sim \sigma_s$ spacing, resulting in cuboidal voxels. Then, for each voxel we identify the neighboring (typically ~ 60) bonded and swelling particles lying inside a 216-voxel cuboid. We diagonalize the corresponding ordering matrix to obtain the voxel degree of order, s_k, and the corresponding director $\mathbf{n}_k$. The voxel is then colored according to the color-coding used for traditional snapshots. Its brightness is scaled quadratically between the lowest possible s_k value, -0.5, and the highest value found in the snapshot. Hence, dark areas reveal the locus of topological disclinations, identified by $s_k < 0.3$. — Coarse-graining is also useful to identify orientational domains and determine their properties. As domains take rather complex shapes, from each voxel we perform a recursive walk on the cubic mesh to identify all neighboring voxels whose directors satisfy $(\mathbf{n}_k \cdot \mathbf{n}_j)^2 > 0.9$ and $s_k > 0.3$ (i.e., are nearly mutually parallel and well-ordered). The actual number of domain molecules (n) is estimated by dividing the domain volume by $\sigma_s^3/\rho^* \approx 3.48\,\sigma_s^3$, i.e., the average volume occupied by a single molecule. Note that this procedure assigns a domain to each voxel and that the domains pertaining to neighboring voxels heavily overlap. For molecules within each domain, an orientational order parameter is calculated as described above, to yield (after averaging over voxels) the domain order parameter S_d.

4 Results

4.1 Zero-stress ground state and temperature scans

We first explore the behavior of the prepared LCE samples as the temperature is varied. A typical MC run at a given temperature starts from the initially cubic reference sample (or, alternatively, from an already relaxed sample at a nearby temperature), allowing its sides to change under zero external stress while conserving the volume. Here, releasing the simulation box side constraints is essential to obtain only orientational domains originating in polymer network irregularity and to avoid those possibly created as a spurious finite-size effect. From our preliminary simulations we find that the sample containing 216000 monomers (with a typical sample side approaching $\sim$ 50 nm if $\sigma_s = 0.5$ nm) is the smallest that can still be considered as polydomain. In smaller samples the parallel aligning tendency of the mesogens, together with the bending rigidity of polymer strands, overcomes the disorder induced by the irregular polymer network, and these samples, if free to relax, adopt an elongated shape with an ordered domain distribution. This is not really surprising as in real polydomain materials the (micrometric) domain size significantly exceeds the (nanometric) distance between the crosslinks, and model samples should approach this.

Typical molecular snapshots for different values of reduced temperature T^* are displayed in Figure 1 (c-e) for the $N = 216000$ sample. The colored particles belong to the polymer network (red, green, and blue color-code alignment along x, y, and z, respectively), while their grey counterparts are the swelling monomers. No significant phase separation is observed. At $T^* = 3.0$ the elastomer is in the orientationally ordered nematic phase featuring several domains with different director orientation. Cooling the system to $T^* = 1.0$, positional order — smectic layering — occurs in addition to the orientational one. Heating instead the sample from $T^* = 3.0$, the degree of orientational ordering is at first reduced, and at $T^* = 7.0$ all ordering appears to be lost — here the LCE is in the isotropic phase. These observations are consistent with the coarse-grained snapshots drawn in Figure 1 (f-h). The

color-coding is the same as for traditional snapshots, while the brightness increases with the degree of orientational order. In the orientationally ordered low-temperature phases the dark spots correspond to regions where the nematic director is not well-defined, i.e., to topological defects. An example of such a defect is highlighted by the dashed circles in Figure 1 (c,f).

More quantitatively, a temperature scan of the heat capacity (obtained from internal energy fluctuations) is shown in Figure 2. It exhibits two anomalies, which suggests the existence of two phase transitions: the nematic-isotropic (NI) at $T^*_{NI} \approx 5.5 \pm 0.5$ and the smectic-nematic (SN) at $T^*_{SN} \approx 1.5 \pm 0.5$. In comparison with transition temperatures observed in simulated regular monodomain samples ($T^*_{NI} \approx 6.25 \pm 0.25$ and $T^*_{SN} \approx 2.0 \pm 0.5$ for $N = 8000$),[28] here both transitions have moved towards lower T^*. Note that the regular and the present irregular samples strongly differ in polymer network architecture and that the shift of transition temperatures (at a given system size) could be attributed to the presence of more significant network disorder in the present case.

Liquid-crystalline systems are characterized by an orientational order parameter that at microscopic level is defined as $S = [3\langle(\mathbf{u}_i \cdot \mathbf{n})^2\rangle_i - 1]/2$. Here the unit vectors $\mathbf{u}_i$ and $\mathbf{n}$ correspond to the long axes of the constituent uniaxial particles (ellipsoids) and to the director, respectively, and $\langle\cdots\rangle_i$ denotes an average over particles. Perfect orientational order yields $S = 1$, complete disorder (isotropy) $S = 0$. In a monodomain system $\mathbf{n}$ and S are uniform across the sample. Polydomain systems, instead, are characterized by a static or quasi static distribution of ordered domains, each consisting of a cluster of particles (here bonded and swelling monomers) that tend to be parallel to a local director $\mathbf{n}_L$, with a local nematic order parameter S_L.[1] One can also consider the overall ("global") order parameter S_G calculated across all domains, together with a global director $\mathbf{n}_G$. In the case of uniaxial molecular ordering one has $S_G \approx S_L S_n$ (following from the addition theorem for spherical harmonics), where $S_n = [3\langle(\mathbf{n}_L \cdot \mathbf{n}_G)^2\rangle - 1]/2$ is an order parameter of $\mathbf{n}_L$ with respect to the global $\mathbf{n}_G$, the average $\langle\cdots\rangle$ being performed over domains. Hence, S_n measures the overall anisotropy of the local director distribution in space. Thus an isotropic polydomain sample

with $S_n \approx 0$ will exhibit global disorder ($S_G \to 0$), due to random orientations of domain directors, even if $S_L \neq 0$. On the contrary, in monodomain systems $S_n \to 1$ and there is only little difference between S_G and S_L.[28] Experimentally, S_G could be measured, e.g., from the dielectric or magnetic susceptibility anisotropy of the sample, while S_L should be accessible, e.g., by magnetic resonance (nuclear[57] or electron spin[58]).

The temperature dependences of S_G and S_L are shown in Figure 2, *bottom*. As expected, in the isotropic phase above T^*_{NI} both parameters approach zero — there is neither global nor local orientational order. In the ordered nematic and smectic phases, S_L increases upon cooling, reflecting the increase of local molecular alignment. We see, however, that in this temperature range also the global S_G takes nonzero (even if relatively small) values and, especially at nematic temperatures, the two curves are essentially scaled by a fairly constant value of S_n. At $T^* = 3.0$ in particular we have $S_n \approx 0.26$, which is a residual albeit small finite-size effect. The nonzero S_n values turn out to decrease with increasing sample size, which confirms that our genesis procedure is not intrinsically biased and can indeed generate isotropic polydomains. This is further demonstrated by the temperature dependence of the reduced simulation box sides (λ_x, λ_y, and λ_z), normalized with respect to those of the reference sample. In the isotropic phase their values approach ~ 1, but in the orientationally ordered nematic and smectic phases a weak spontaneous elongation along the y-axis is seen (Figure 2, *center*). This elongation ($\sim 17\%$ at $T^* = 3.0$) is intimately related with the residual global order via the strain-alignment coupling and decreases with increasing system size, too.

These observations agree with the snapshots plotted in Figure 3 at zero stress and $T^* = 3.0$ in the nematic phase. Our $N = 216000$ sample appears as an almost fully isotropic polydomain; see Figure 3 (a). A more quantitative analysis reveals only a slight net molecular alignment, with $\mathbf{n}_G$ along y, resulting in $S_G \approx 0.14$. In phenomenological terms, a rather weak aligning mechanical field has been established along y. The domain shapes are rather irregular and, in part, also percolating. An average domain contains $\langle n \rangle \sim 10^4$ GB ellipsoids,

while the largest domains are as large as 2.4×10^4 particles.The almost isotropic nature of our sample is further confirmed by the rather isotropic shape of the polymer strand end-to-end vector probability distribution at zero stress, Figure 3 (b). We notice that the boundaries between domains — although not very well defined — are often accompanied by the presence of topological defect lines (disclinations) visualized in Figure 3 (c). The rather complex defect structure mainly consists of $\pm 1/2$-strength disclinations [see Figure 1 (c,f)], the least costly in free energy.[59] Note also that "checkerboard" domain patterns and oscillatory orientational correlations observed experimentally and predicted theoretically at the micron-scale[35,60,61] seem to be absent in our still relatively small system.

4.2 Stress-strain behavior

To explore the intriguing possibility of achieving soft elastic deformations that require a relatively small amount of work, stress-strain virtual experiments with the $N = 216000$ sample were carried out in the nematic phase at $T^* = 3.0$. External stress (σ^* in reduced units) is applied by pulling along the z-axis — perpendicular to the residual nematic director $\mathbf{n}_G$ and the self-established mechanical aligning field. The corresponding snapshots are shown in Figure 3, and the engineering stress vs. strain curve (a common presentation for experimental work) in Figure 4, *top*. Qualitatively, the curve looks similar to those shown by experiments on I-PDE:[35,40,42] it exhibits a narrow initial region of small elongation when low stress is applied, then a very soft region where a major elongation of more than 200% is obtained with a small increase of stress, and a third region where the LCE stiffens and high stress is required for further elongation.[1] In the first low-stress region, the large sample deforms only slightly ($\sim 20\%$), with a Young elastic modulus (estimated from the curve slope) around $E \sim 300$ kPa. Then, after the weak perpendicular mechanical field has been overcome at around $\sigma^* \sim 0.005$ (corresponding to ~ 55 kPa), the slope is significantly reduced and the curve exhibits a slightly tilted plateau with $E \sim 100$ kPa, until a deformation of $\sim 200\%$ is reached. Then, the elastomer becomes significantly stiffer and the Young

modulus reaches several MPa towards the end of the simulated curve. The total work density needed to achieve a 200% deformation (proportional to $\int \sigma^* \mathrm{d}\lambda_z$ and deduced from the stress-strain curve) that takes the sample across the polydomain-monodomain (PM) transition is estimated as < 300 kJm^{-3}. In our experience larger samples enter the plateau at a lower stress value than the smaller ones because they are characterized by weaker global order and, consequently, by a weaker built-in mechanical field to be overcome.

5 Discussion

Different microscopic mechanisms can be conceived to explain the PM transition, including (i) domain rotation, (ii) domain growth, (iii) order destruction, and (iv) quake-like release of local tension, that we now consider in turn. (i) *Domain rotation.* In this case each of the isotropically distributed domains would behave independently and simply rotate when the sample is stretched.[1,33] The global order parameter S_G would start from a small value and, at the end of the process, approach the original local S_L, while the average domain size $\langle n \rangle$ (here expressed through the number of domain monomers, n) would remain essentially unchanged. (ii) *Domain growth.* Another possibility is that the domains that already happen to be oriented along the stretching direction grow, helped by the correlation between the local domains. In this case S_G should grow together with an increase of $\langle n \rangle$. There is some evidence that (i) and (ii) can be combined.[40,45] (iii) *Order destruction.* An alternative, totally different, mechanism could proceed through a destruction of existing local order, followed by a reconstruction of the alignment along the new mechanical field-imposed direction. (This could be due to the difficulty of rotating domains, e.g., due to crosslinks.) A similar process was observed by computer simulations when trying to align the secondary director of a monodomain biaxial LC with a field perpendicular to its initial orientation.[62] In this case the initial and final degree of local (S_L) and domain (S_d) order are expected to be comparable, while the intermediate state should be characterized by a significant decrease of S_L and S_d.

(iv) *Quake-like release of local tension.* Yet another mechanism [accompanying (i) and (ii)] could rely on the unavoidable presence of an excess of elastic free energy stored by topological defects when domains with different local directors clash together.[1] Upon stretching above a certain threshold, this free energy could suddenly be released as domains rotate and/or grow, reducing the defect volume fraction, in a sort of irreversible[40,44] quake.

Figure 4, *bottom*, shows the average domain size $\langle n \rangle$ plotted against stress. Below the stress-strain plateau, $\langle n \rangle$ at first drops very slightly, while the domain size distribution shape is largely unaffected by stretching. The accompanying weak sample elongation seems to be mainly due to molecular reorientation, as suggested by the order parameter S_z (measuring orientational order with respect to the externally fixed stretching direction, z-axis) that already exhibits a certain increase in this σ^* range (Figure 4, *center*). Qualitatively, a similar conclusion can be made by comparing the domain patterns in snapshots for $\sigma^* < 0.005$. Note that $S_z < 0$ indicates that we initially pull perpendicular to $\mathbf{n}_G$. Once the stress-strain plateau is reached, both $\langle n \rangle$ and S_z swiftly increase, which suggests a simultaneous major reorientation and merging of domains. Above the plateau ($\lambda_z > 3$, $\sigma^* > 0.04$) $\langle n \rangle$ and S_z saturate, and the sample has now become a rather well-aligned elongated monodomain with $\langle n \rangle \to N$ and $S_z > 0$. This is suggested by the snapshots, as well as by the polymer chain end-to-end spatial distribution isosurfaces, Figure 3 (b): upon pulling, the initially rather isotropic polydomain distribution gradually evolves into a prolate monodomain one.

On the central plate of Figure 4 we also show (empty circles) the S_z versus σ^* dependence for the short cross-linker groups, i.e. the length-one chains [cf. Figure 1 (b)]. Since this dependence follows closely that calculated for all mesogens over the entire σ^* range, on stretching these linkers appear to reorient together with the surrounding mesogenic material, rather than keeping their initial quenched orientations. At the same time, across the PM transition, local nematic ordering is well-maintained. This can be concluded from the stress dependence of the local order parameter S_L that is also plotted in Figure 4, *center*. It starts from $S_L \sim 0.56$ at zero stress and is monotonically enhanced to ~ 0.79 on increasing σ^*.

In the same plot, the domain orientational order parameter S_d is also presented, exhibiting similar behavior as S_L.

In a stretching experiment, domain reorientation and growth are accompanied by the reduction of the total disclination line length. Apart from observing this trend from snapshots, Figure 3 (c), it can be roughly deduced by calculating the volume fraction ϕ_d occupied by the disclinations. (The disclination diameter is determined by the nematic correlation length and should not vary significantly along a disclination.) The ϕ_d versus σ^* dependence is shown in Figure 4, *bottom*, and is indeed intimately related to the $\langle n \rangle$ dependence.

It also appears that within and above the supersoft plateau our samples are characterized by pronounced memory effects. On stress removal, they will typically not return to their initial shape and the achieved elongation will decrease only slightly, which is similar to the behavior observed in some experimental main-chain systems.[40,44] Only transient perturbations resulting in minor (a few %) deformations turn out to be almost completely reversible.

The stress-strain behavior of the PM transition obtained from our simulations is phenomenologically similar to that predicted theoretically in non-ideal supersoft LCE: The supersoft plateau is entered only beyond a stress threshold associated with a symmetry-breaking intrinsic mechanical field tending to vanish when increasing sample size. In our case the behavior may not be completely soft in the sense of the neo-classical rubber elastic theory,[1,34] suggesting pure domain rotation, whereby the polymer chain end-to-end distribution is rotated but otherwise maintains its structure. Given the complicated shape of our domains, on the plateau we seem to observe combined domain growth and rotation. At the same time we can exclude any destruction of local orientational order, as observed, e.g., in Ref.[62] At the end of the plateau, the aligning process has been very thorough and has apparently reoriented even the possible sources of quenched disorder reminiscent of the initial polydomain pattern. For this reason, the observed stress-strain behavior is irreversible and features memory effects. This irreversibility and the removal of disclinations upon stretching

are also compatible with the occurrence of microquakes; however, in our simulations we have been unable to observe any of them directly, as, for computational reasons, each stress-strain data point is obtained in a separate run, rather than by gradually increasing stress.

LCE response in a stretching experiment is never immediate and therefore the resulting stress-strain curves may depend on the experimental time-window.[63] Here great care is taken to relax our samples, but of course a further evolution, especially within the plateau region, cannot be excluded. The equilibrium stress-strain curve can also be estimated from the exponential fits of the λ_z MC-"time" evolution for each σ^* and compared with the dataset available directly from simulation after $\sim 52 \times 10^6$ MC cycles, shown in Figure 4. The soft plateau-like region is observed in both cases.

So far most of the polydomain LCE experimental data has been obtained either in nematic side-chain or in smectic main-chain systems. Many features of our system agree also with those of the latter, e.g., the stress-strain curve shape with a slightly tilted plateau (including, very approximately, the corresponding Young moduli[42]) and its irreversibility.[40–42,44] Our stress-strain curves are also similar to those reported for reversible nematic side-chain systems,[35,39] but are not so soft, being characterized by a higher plateau threshold stress σ_c^*. This comes to terms with the theoretical prediction that σ_c^* is larger in the more anisotropic main-chain LCE.[33] Together with a much longer stress-strain plateau in main-chain LCE, this results in a higher amount of work necessary to carry out the PM transition. Note also that the values of Young moduli and mechanical work reported above sensitively depend on particle size σ_s, all scaling as $\propto 1/\sigma_s^3$. For simplicity, our ellipsoidal particles (bonded and swelling) are assumed all equal, and taking $\sigma_s = 0.5$ nm results in ellipsoids as short as 1.5 nm. In reality, bonded molecules can be larger than this, which would noticeably decrease the estimated moduli and work densities.

Our crosslinked elastomeric systems are characterized by a non-negligible presence of swelling monomers. Previous work[28,30] has shown that at monomer concentrations considered here no significant phase separation is observed, and that the nematic-isotropic

transition, strain-alignment coupling, and actuation response are qualitatively similar to those observed in homogeneous systems. Therefore, we believe that the presence of swelling monomers does not significantly affect any of our results, and we expect them to apply both to swollen and dry LCE.

6 Conclusion

In conclusion, we have analyzed the molecular mechanism underlying the supersoft elasticity in polydomain LCE. First, we have developed a computer simulation method to generate polydomain LCE in the isotropic phase and applied it to swollen main-chain systems obtained by polymerizing and cross-linking ellipsoidal monomer beads interacting with a soft variant of the Gay-Berne potential. Then, we have performed large-scale iso-stress molecular Monte Carlo simulations of the poly-to-monodomain transition for a 216000 particle system, reproducing the characteristic soft-elasticity plateau in the stress-strain behavior. Our sample preparation protocol — given a sufficiently large system size — produces an isotropic elastomer network, representing the so-called isotropic phase-generated polydomain LCEs.[35] A detailed analysis of the results shows that the polydomain-monodomain transition does not take place via an order destruction-reconstruction mechanism, but rather that it is characterized by simultaneous domain growth and rotation, and is assisted by defect coarsening-out elastic energy release.

7 Acknowledgement

The financial support from the Slovenian Research Agency and the European Union (Programme P1-0099 and NAMASTE Center of Excellence) is acknowledged. We also thank the ARCTUR d.o.o. company (`www.arctur.si`) and the Space-SI Center of Excellence for sharing their computational resources, as well as Simon Čopar for help with isosurface visualization. C.Z. thanks MIUR–PRIN project *"Novel ordered systems for high response*

molecular devices" (2009N5JH4F) for financial support, and the Isaac Newton Centre, Cambridge, UK, for hospitality that lead to many stimulating discussions during the program "The Mathematics of Liquid Crystals".

References

(1) Warner, M.; Terentjev, E. M. *Liquid Crystal Elastomers, 2nd Edition*, Oxford University Press: Oxford, 2007.

(2) Torras, N.; Zinoviev, K. E.; Esteve, J.; & Sánchez-Ferrer, A. *J. Mat. Chem. C* **2013**, *1*, 5183-5190.

(3) Ohm, C.; Brehmer. M.; Zentel, R. *Adv. Mater.* **2000**, *22*, 3366-3387.

(4) Ohm, C.; Haberkorn, N.; Theato, P.; Zentel. R. *Small* **2011**, *7*, 194-198.

(5) Fleischmann. E. K.; Ohm, C.; Serra. C.; Zentel, R. *Macromol. Chem. and Phys.* **2012**, *213*, 1871-1878.

(6) Jiang, H.; Lia, C.; Huanga, X. *Nanoscale* **2013**, *5*, 5225-5240.

(7) Urayama, K. *React. Funct. Polym.* **2013**, *73*, 885-890.

(8) Agrawal, A.; Chipara, A. C.; Shamoo, Y.; Patra, P. K.; Carey, B. J.; Ajayan, P. M.; Chapman, W. G.; Verduzco, R. *Nat. Commun.* **2013**, *4*, doi: 10.1038/ncomms2772.

(9) Spillmann, C. A.; Naciri, J.; Martin, B. D.; Farahat, W.; Herr, H.; Ratna, B. R. *Sensors and Actuators A* **2007**, *133*, 500-505.

(10) Li, M. H.; Keller, P. *Phil. Trans. Roy. Soc. A* **2006**, *364*, 2763-2777.

(11) Madden, J. D. W; Vandesteeg, N. A.; Anquetil, P. A.; Madden, P. G. A.; Takshi, A.; Pytel, R. Z.; Lafontaine, S. R.; Wieringa, P. A.; Hunter, I. W. *IEEE J Oceanic Eng.* **2004**, *29*, 706-728.

(12) Mirfakhrai, T.; Madden, J. D. W; Baughman, R. H., *Materials Today* **2007** *10*, 30-38.

(13) Buguin, A.; Li, M. H.; Silberzan, P.; Ladoux, B.; Keller, P. *J. Am. Chem. Soc.* **2006**, *128*, 1088-1089.

(14) Marshall, J. E.; Gallagher, S.; Terentjev, E. M.; Smoukov, S. K. *J. Am. Chem. Soc.* **2014**, *136*, 474-479.

(15) Fleischmann, E. K.; Liang, H. L.; Kapernaum, N.; Giesselmann, F.; Lagerwall, J.; Zentel, R. *Nat. Commun.* **2012**, *3*, doi: 10.1038/ncomms2193.

(16) Cui, J.; Drotlef, D.-M.; Larraza, I.; Fernández-Blázquez, J. P.; Boesel, L. F.; Ohm, C.; Mezger, M.; Zentel, R.; del Campo, A. *Adv. Mater.* **2012**, *24*, 4601-4604.

(17) Torras, N.; Zinoviev, K. E.; Camargo, C. J.; Campo, E. M.; Campanella, H.; Esteve, J.; Marshall, J. E.; Terentjev, E. M.; Omastova, M.; Krupa, I.; Teplicky, P.; Mamojka, B.; Bruns, P.; Roeder, B.; Vallribera, M.; Malet, R.; Zuffanelli, S.; Soler, V.; Roig, J.; Walker, N.; Wenn, D.; Vossen, F.; Crompvoets, F. M. H. *Sens. Actuator A-Phys.* **2014**, *208*, 104-112.

(18) Camacho-López, M.; Finkelmann, H.; Palffy-Muhoray, P.; Shelley, M. *Nature Mat.* **2004**, *3*, 307-310.

(19) Amigo-Melchior, A.; Finkelmann, H. *Polymers for Advanced Technologies* **2002**, *13*, 363-369.

(20) Castles, F.; Morris, S. M.; Hung, J. M. C.; Qasim, M. M.; Wright, A. D.; Nosheen, S.; Choi, S. S.; Outram, B. I.; Elston, S. J.; Burgess, C.; Hill, L.; Wilkinson, T. D.; Coles, H. J. *Nature Mat.* **2014**, doi: 10.1038/nmat3993.

(21) Hiscock, T.; Warner, M.; Palffy-Muhoray, P. *J. Appl. Phys.* **2011**, *109*, 104506.

(22) de Gennes, P.-G. *C. R. Acad. Sc. Paris* **1975**, *281*, 101-103.

(23) Küpfer, J.; Finkelmann, H. *Macromol. Chem. Rapid Commun.* **1991**, *12*, 717-726.

(24) Bladon, P.; Terentjev, E. M.; Warner, M. *Phys. Rev. E* **1993**, *47*, R3838-R3840.

(25) DeSimone, A.; Dolzmann, G. *Arch. Ration. Mech. Anal.* **2002**, *161*, 181-204.

(26) Darinskii, A. A.; Zarembo, A.; Balabaev, N. K.; Neelov, I. M.; Sundholm, F. *Macromol. Symp.* **2006**, *237*, 119-127.

(27) Darinskii, A. A.; Zarembo, A.; Balabaev, N. K. *Macromol. Symp.* **2007**, *252*, 101-109.

(28) Skačej, G.; Zannoni, C. *Soft Matter* **2011**, *7*, 9983-9991.

(29) Ilnytskyi, J. M.; Saphiannikova, M.; Neher, D.; Allen, M. P. *Soft Matter* **2012**, *8*, 11123-11134.

(30) Skačej, G.; Zannoni, C. *Proc. Natl. Acad. Sci. USA* **2012**, *109*, 10193-10198.

(31) Fridrikh, S. V.; Terentjev, E. M. *Phys. Rev. Lett.* **1997**, *79*, 4661-4664.

(32) Yu, Y. K.; Taylor, P. L.; Terentjev, E. M. *Phys. Rev. Lett.* **1998**, *81*, 128-131.

(33) Fridrikh, S. V.; Terentjev, E. M. *Phys. Rev. E* **1999**, *60*, 1847-1857.

(34) Warner, M.; Bladon, P.; Terentjev, E. M. *J. Phys. II* **1994**, *4*, 93-102.

(35) Urayama, K.; Kohmon, E.; Kojima, M.; Takigawa, T. *Macromolecules* **2009**, *42* 4084-4089.

(36) Biggins, J. S.; Warner, M.; Bhattacharya, K. *Phys. Rev. Lett.* **2009**, *103*, 037802.

(37) Biggins, J. S.; Warner, M.; Bhattacharya, K. *J. Mech. Phys. Solids* **2012**, *60*, 573-590.

(38) Uchida, N. *Phys. Rev. E* **2000**, *62*, 5119-5136.

(39) Higaki, H.; Urayama, K.; Takigawa, T. *Macromol. Chem. Phys.* **2012**, *213*, 1907-1912.

(40) Ortiz, C.; Wagner, M.; Bhargava, N.; Ober, C. K.; Kramer, E. J. *Macromolecules* **1998**, *31*, 8531-8539.

(41) Giamberini, M.; Cerruti, P.; Ambrogi, V.; Vestito, C.; Covino, F.; Carfagna, C. *Polymer* **2005**, *46*, 9113-9125.

(42) Sánchez-Ferrer, A.; Finkelmann, H. *Macromol. Rapid Commun.* **2011**, *32*, 309-315.

(43) Tokita, M.; Tagawa, H.; Niwano, H.; Sada, K.; Watanabe, J. *Jpn. J. Appl. Phys.* **2006**, *45*, 1729-1733.

(44) Ishige, R.; Osada, K.; Tagawa, H.; Niwano, H.; Tokita, M.; Watanabe, J. *Macromolecules* **2008**, *41*, 7566-7570.

(45) Whitmer, J. K.; Roberts, T. F.; Shekhar, R.; Abbott, N. L.; de Pablo, J. J. *Phys. Rev. E* **2013**, *87*, 020502.

(46) Zentel, R. *Liq. Cryst.* **1986**, *1*, 589-592.

(47) Berardi, R.; Zannoni, C.; Lintuvuori, J. S.; Wilson, M. R. *J. Chem. Phys.* **2009**, *131*, 174107-174112.

(48) Gay, J. G.; Berne, B. J. *J. Chem. Phys.* **1981**, *74*, 3316-3319.

(49) Berardi, R.; Emerson, A. P. J.; Zannoni, C. *J. Chem. Soc. Faraday Trans.* **1993**, *89*, 4069-4078.

(50) Bird, R. B.; Armstrong, R. C.; Hassager, D. *Dynamics of Polymeric Liquids*, J. Wiley: New York, 1971.

(51) Berardi, R.; Micheletti, D.; Muccioli, L.; Ricci. M.; Zannoni, C. *J. Chem. Phys.* **2004**, *121*, 9123-9130.

(52) Micheletti, D.; Muccioli, L.; Berardi, R.; Ricci, M.; Zannoni, C. *J. Chem. Phys.* **2005**, *123*, 224705.

(53) Frenkel, D.; Smit, B. *Understanding Molecular Simulation: From Algorithms to Applications*, Academic Press: San Diego, 1996.

(54) Verlet, L. *Phys. Rev.* **1967**, *159*, 98-103.

(55) Allen, M. P.; Tildesley, D. J. *Computer Simulations of Liquids*, Clarendon Press: Oxford, 2000.

(56) Barker, J. A.; Watts, R. O. *Chem. Phys. Lett.* **1969**, *3*, 144-145.

(57) Domenici, V. *Prog. NMR Spectr.* **2012**, *63*, 1-32.

(58) Zannoni, C.; Pedulli, G. F.; Masotti, L.; Spisni, A. *J. Mag. Res. A* **1981**, *43*, 141-153.

(59) Chaikin, P. M.; Lubensky, T. C. *Principles of Condensed Matter Physics*, Cambridge University Press: Cambridge, 1997.

(60) Lu, B.-S.; Ye, F.; Xing, X.; Goldbart, P. M. arXiv:1101.1323v1 [cond-mat.soft], 2011.

(61) Lu, B.-S.; Ye, F.; Xing, X.; Goldbart, P. M. *Phys. Rev. Lett.* **2012**, *108*, 257803.

(62) Berardi, R.; Muccioli, L.; Zannoni, C. *J. Chem. Phys.* **2008**, *128*, 024905.

(63) Clarke, S. M.; Terentjev, E. M. *Phys. Rev. Lett.* **1998**, *81*, 4436-4439.

Graphical TOC Entry

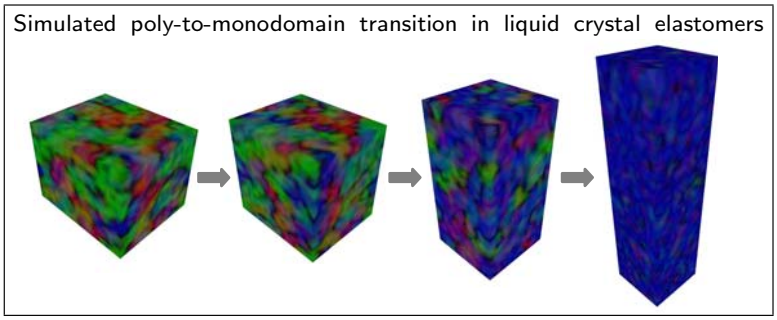

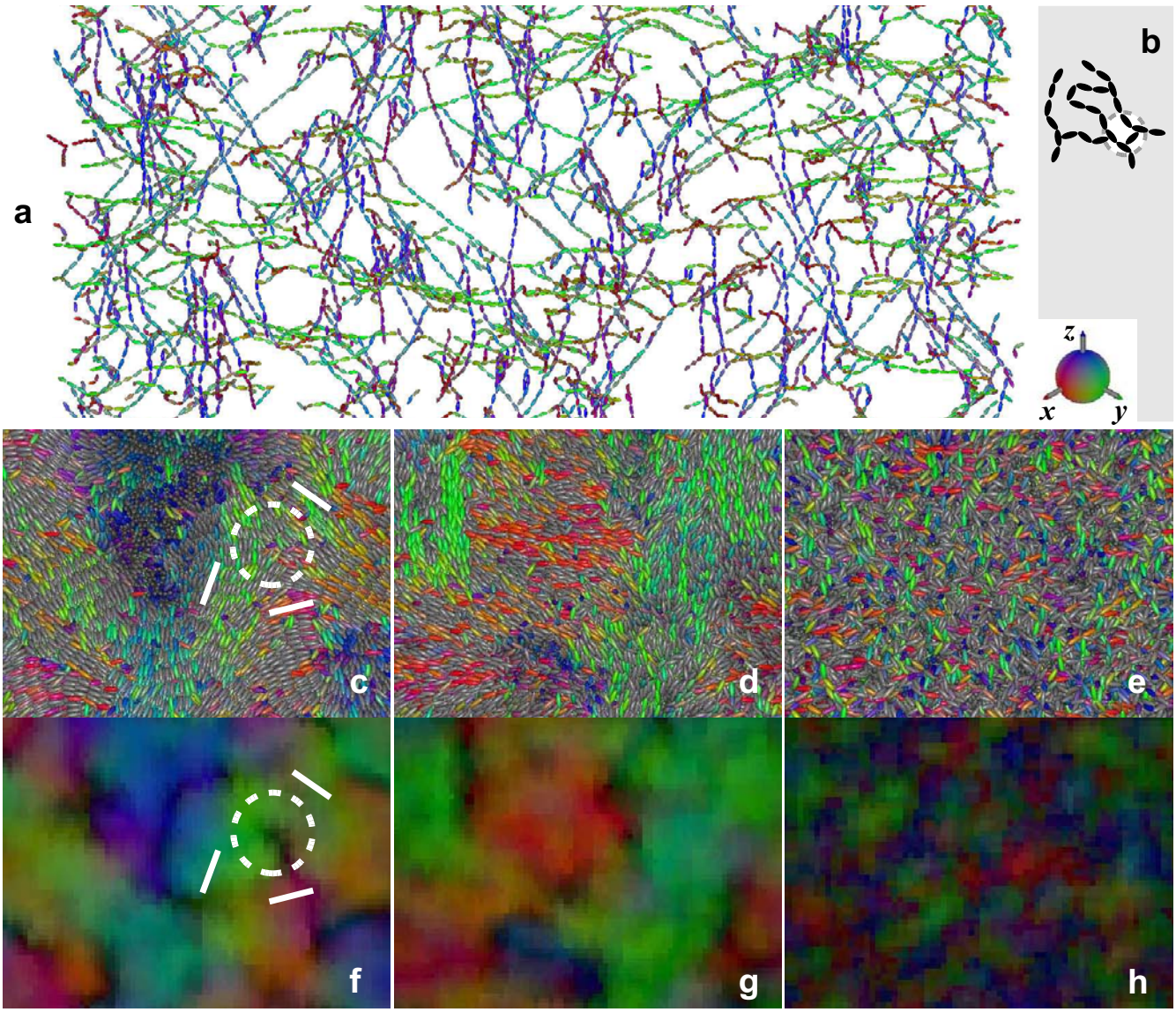

Figure 1: Simulated elastomer network: (a) snapshot of a thin elastomer slice after a negative pressure shock revealing network topology and (b) a particular where the dashed circle features a difficult-to-reorient cross-linked molecular group potentially acting as a source of quenched orientational disorder. Zero-stress sample snapshots (c-e) and their coarse-grained visualizations (f-h): smectic at $T^* = 1.0$ (c,f), nematic at $T^* = 3.0$ (d,g), and isotropic phase at $T^* = 7.0$ (e,h). Bonded monomer orientations along x, y, and z are color-coded as red, green, and blue, respectively (see color palette); nonbonded monomers are shown in grey. Bright and dark regions in the coarse-grained snapshots correspond to high and low degree of orientational order, respectively. The dashed circle in plates (c,f) highlights one of the $-1/2$-strength disclinations, while the three straight lines represent the local directors $\mathbf{n}_L$ of the nearby domains.

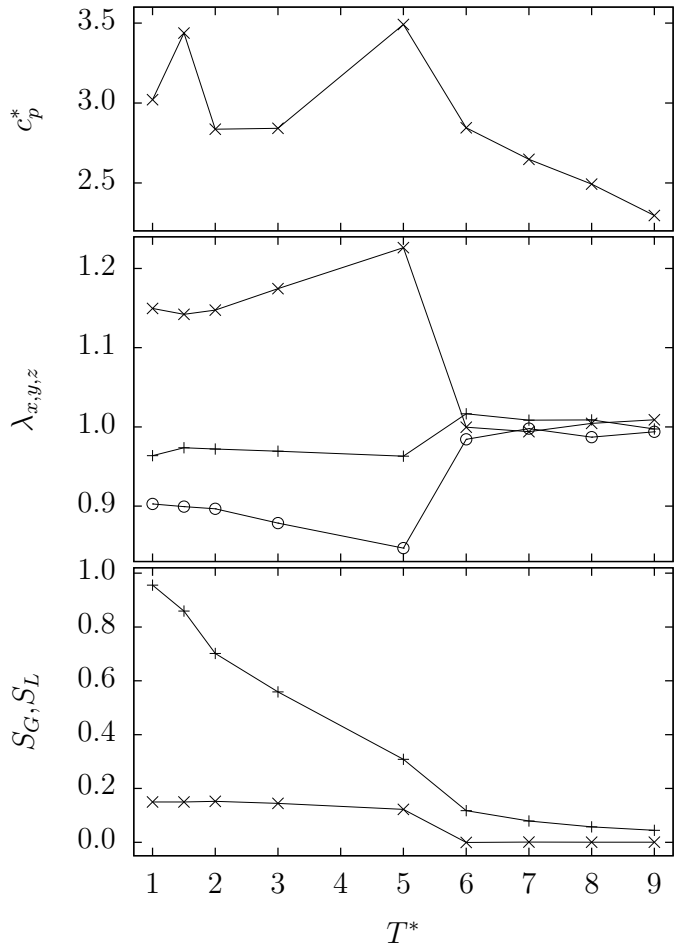

Figure 2: Zero-stress temperature scans. *Top:* reduced heat capacity (per particle and in units of k_B), *center:* reduced simulation box sides (normalized with respect to those of the reference sample), and *bottom:* global (S_G, $\times$) and local (S_L, $+$) nematic order parameter.

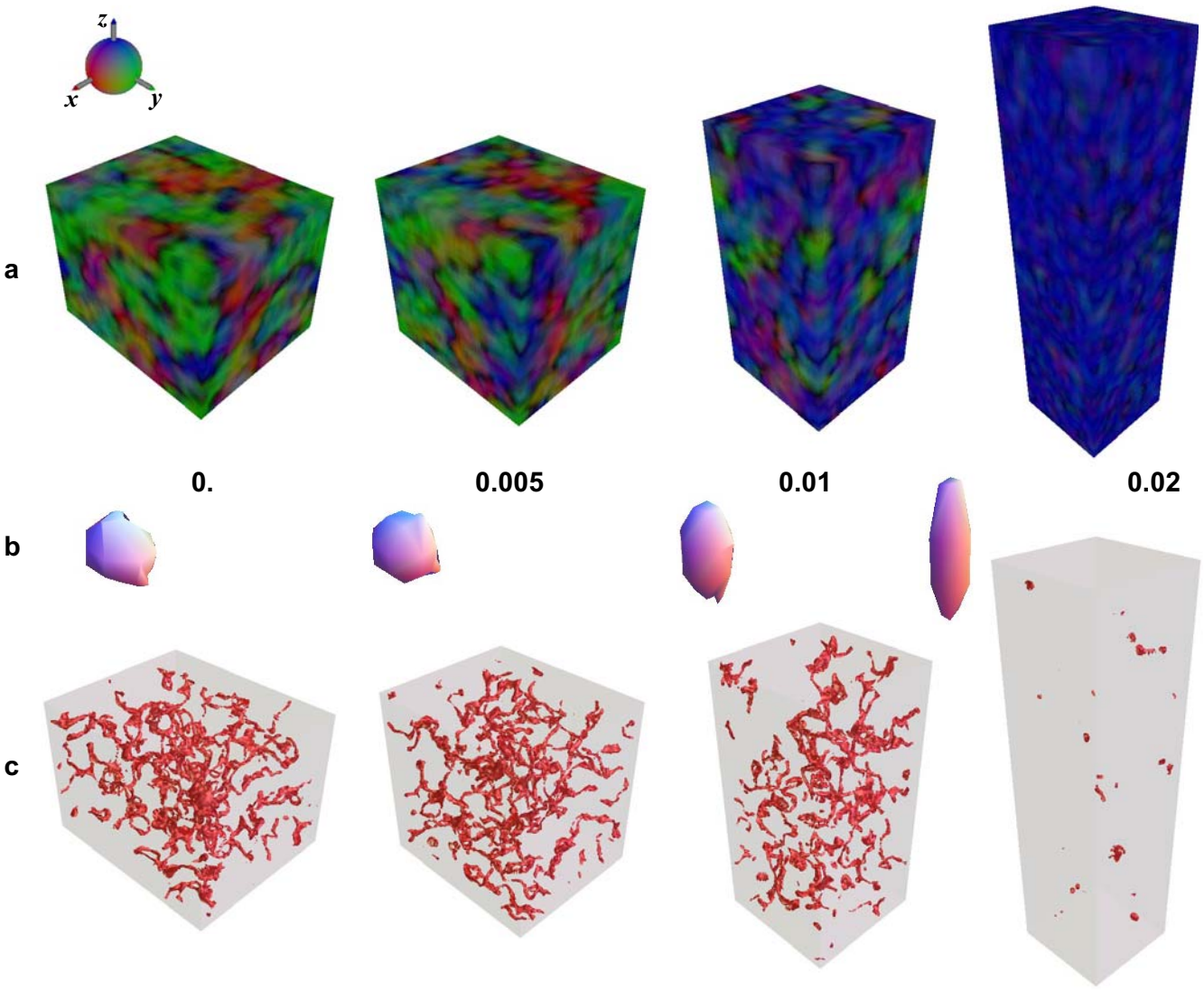

Figure 3: Stress-strain experiment performed at a nematic temperature ($T^* = 3.0$). (a) Coarse-grained snapshots, with the corresponding reduced engineering stress (σ^*) values displayed. (b) Isosurfaces of the polymer chain end-to-end probability distribution and (c) evolution of nematic defect lines upon increasing σ^*. All snapshots are taken after $\sim 52 \times 10^6$ MC cycles.

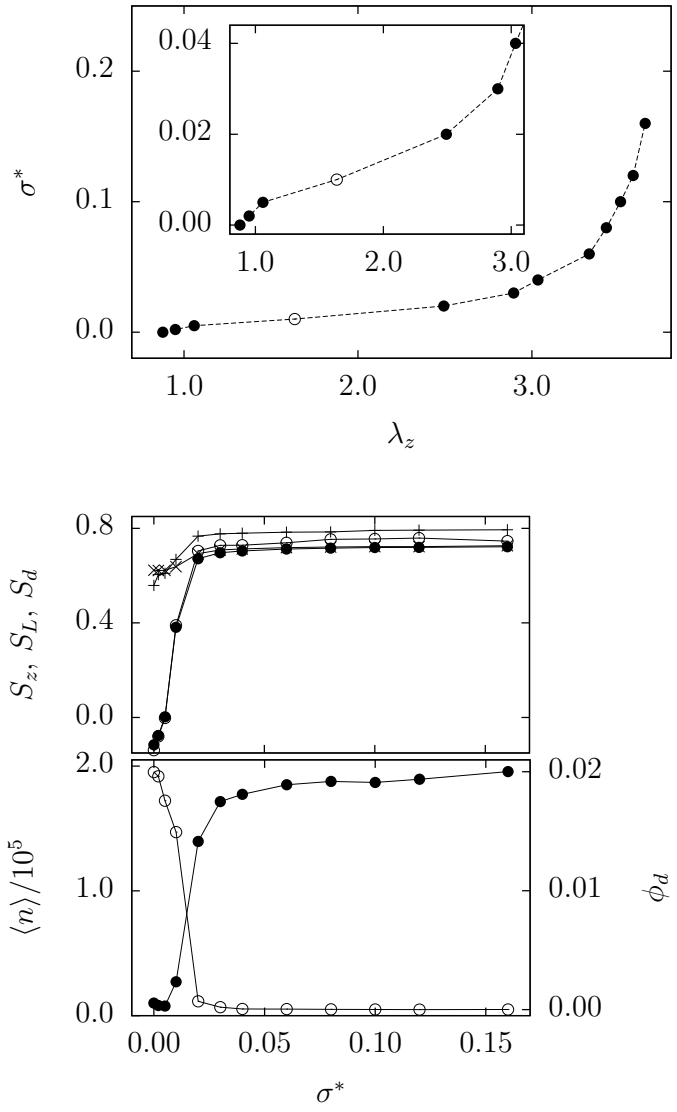

Figure 4: *Top:* Stress-strain curves at $T^* = 3.0$, with low-stress behavior shown as inset. The data collected after ~ 52 MC Mcycles is shown, the empty symbol representing a data point that possibly has not achieved full relaxation. *Center:* Stress dependence of orientational order parameters: S_z calculated for all particles ($\bullet$) and for the crosslinking length-one chains ($\circ$); local S_L ($+$) and domain S_d ($\times$). *Bottom:* Stress dependence of average domain size $\langle n \rangle$ ($\bullet$) and disclination volume fraction ϕ_d ($\circ$). $\sigma^* = 0.01$ approximately corresponds to 110 kPa engineering stress.